LIFTING THE NUCLEAR FOG

J. Pochodzalla,[a] M. Begemann-Blaich,[a] Th. Blaich,[b] H. Emling,[a] A. Ferrero,[c] C. Groß [a] G. Immé,[d] I. Iori,[c] G.J. Kunde,[a] W.D. Kunze,[a] V. Lindenstruth,[a] U. Lynen,[a] T. Möhlenkamp,[e] A. Moroni,[c] W.F.J. Müller,[a] B. Ocker,[f] G. Raciti,[d] T. Rubehn,[a] H. Sann,[a] A. Schüttauf,[f] C. Schwarz,[a] W. Seidel,[e] V. Serfling,[f] J. Stroth,[a] W. Trautmann,[a] A. Trzcinski,[g] A. Tucholski,[g] G. Verde,[d] and A. Wörner,[a] B. Zwieglinski[g] E. Zude,[a]

[a]Gesellschaft für Schwerionenforschung, 64220 Darmstadt, Germany
[b]Institut für Kernchemie, Universität Mainz,55099 Mainz, Germany
[c]Dipartimento di Fisica, Universitá di Milano
and I.N.F.N., 20133 Milano, Italy
[d]Dipartimento di Fisica dell' Universitá
and I.N.F.N., 95129 Catania, Italy
[e]Forschungszentrum Rossendorf, 01314 Dresden, Germany
[f]Institut für Kernphysik,Universität Frankfurt, 60486 Frankfurt
[g]Soltan Institute for Nuclear Studies, 00 681 Warsaw, Hoza 69, Poland

Abstract

Recent results of the ALADIN collaboration are reviewed. Fragment multiplicities and correlations are found to be invariant with respect to a change of the target mass or the beam energy when plotted as a function of Z_{bound}. The dependence of the fragment multiplicity on the projectile mass follows a linear scaling law. For Au+Au reactions at E/A=600 MeV, the mass and the excitation energy of the decaying pre-fragments were determined from the measured fragment and neutron distributions. A temperature scale was derived from observed yield ratios of He and Li isotopes. The relation between this isotope temperature and the excitation energy of the system exhibits a behavior which is expected for a phase transition. The nuclear vapor regime takes over at an excitation energy of 10 MeV per nucleon, a temperature of 5 MeV and may be characterized by a density of 0.15-0.3 normal nuclear density.

1 The Nuclear Paradigm

The prospect of creating a state of matter resembling that of the pre-hadronic phase of the early universe or of the core of today's neutron stars [1] is one of the prime motivations to study relativistic heavy ion collisions. Unquestionable, the transition to the quark-gluon plasma represents the most spectacular example of a phase transition in nuclear matter. The complex structure of the hadronic components and the many facets of their interaction [2], however, offer the opportunity to observe in addition several other, exciting nuclear state transitions (Fig. 1, from ref. [3]). Already two decades ago, the van der Waals behavior of the nucleon - nucleon force inspired the idea of a liquid-gas phase transition in nuclear matter [4,5,6]. What makes this nuclear liquid gas phase transition stand out from all other conceivable nuclear phase transitions

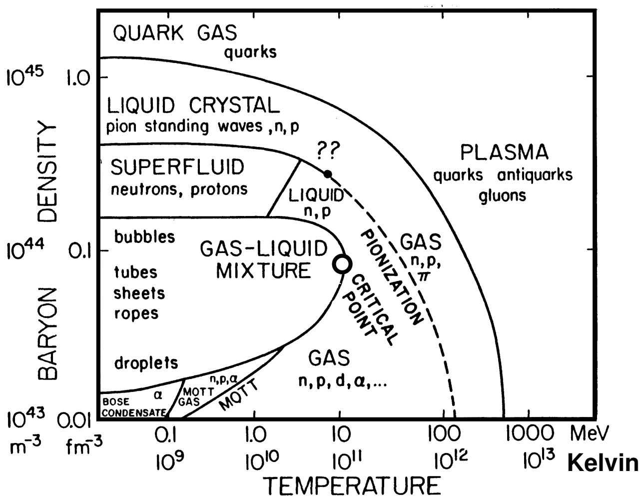

Figure 1: Conceivable landscape of hadronic and nuclear phases [3]. While most regions of this diagram are *terra incognita*, both, the liquid and the gaseous phase of nuclear systems are known to exist.

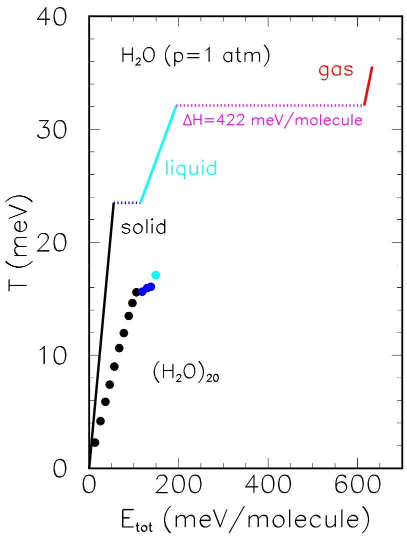

Figure 2: Caloric curve of bulk water at atmospheric pressure (line) and of water clusters consisting of 20 H_2O molecules predicted [22] by molecular dynamics calculations (dots).

though, is the fact that both phases, cold nuclear Fermi liquids on one hand and a nuclear gas consisting of free nucleons and a few light clusters on the other hand, are known to exist in nature, and, what may perhaps be even more important, that both are experimentally accessible. This unique feature makes the nuclear liquid-gas phase transition an ideal and relevant test case for our ability to identify and quantify a phase transition in a finite hadronic system.

The first observation of a self-similar power law for the fragment mass distribution in proton induced reactions was interpreted as an indication for a critical phenomenon [7]. Despite enormous effort during the last decade [8,9,10], the attempts to deduce critical parameters [6] and critical point exponents [11] remained elusive. Searching for signals of a nuclear phase transition, we are facing several complications: Nuclei are composed of a limited number of constituents. In a finite system, fluctuations are limited. Singularities of phase transitions get, therefore, rounded and shifted with respect to their bulk values [12,13]. In addition, the long-range Coulomb-repulsion between the constituent protons introduces instabilities [14,15] which may lead to a further downward shift of the critical temperature [16,17,18]. Since no external fields (e.g. pressure) can be applied to excited nuclei in the laboratory, they may expand prior to their disassembly [19,20]. Eventually, these expanded systems may aggregate into clusters.

Although all these difficulties are inherent for nuclear systems, they do also apply to other fields nuclear physics where finite systems are involved [21]. This is illustrated in

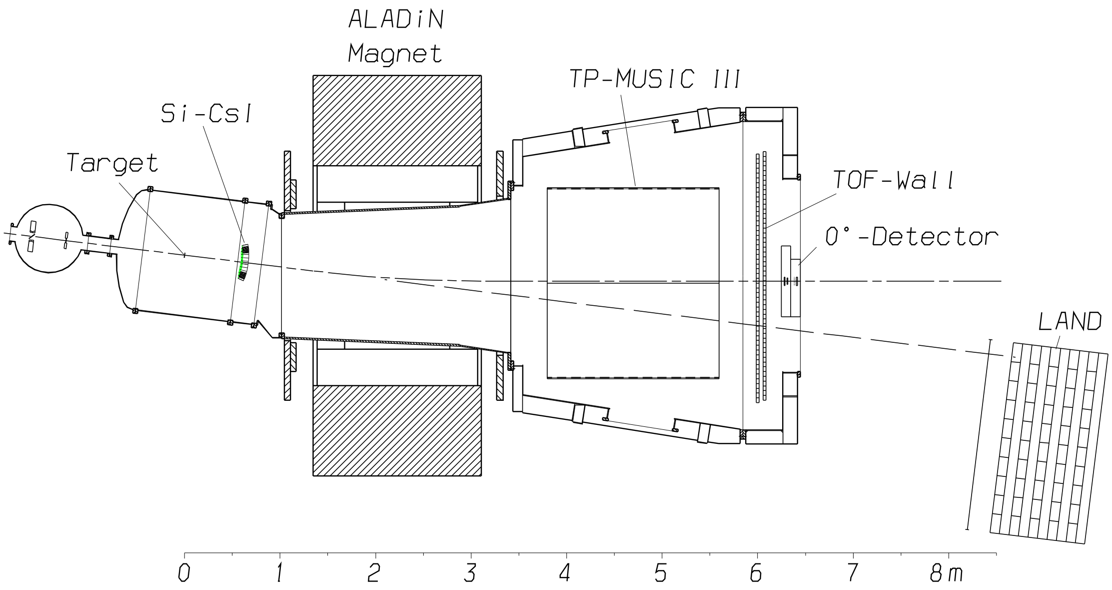

Figure 3: Cross-sectional view of the ALADIN facility. The beam enters from the left and is monitored by the beam counters before reaching the target. The entrance to the dipole magnet is surrounded by the Si-CsI(Tl) array. Projectile fragments are tracked and identified in the TP-MUSIC III detector and in the time-of-flight wall. Coincident neutrons emitted approximately in the direction of the incident beam (dashed line) are detected with the large-area neutron detector (LAND). The dash-dotted line represents the trajectory of beam particles after they were deflected by an angle of 8°.

Fig. 2 for the case of water. The solid line shows the well-known caloric curve of water at normal pressure of 1 atmosphere. Comparing this paradigm of first-order phase transitions to the predicted [22] caloric curve of a finite H_2O cluster (dots in Fig. 2) we recognize the characteristic plateau signaling the solid-to-liquid transition. However, the transition temperature is reduced and distributed over a finite temperature range. Nevertheless, this example illustrates that phase transitions of rather small clusters (~10 constituents) are still well defined, distinguishable [13,23,24,22] and – in case of atomic clusters [25] – even detectable, thus nourishing the hope that nuclear systems produced in energetic heavy ion collisions may also exhibit sufficient clear signatures of a phase transitions.

2 The Making of Boiling Nuclei

Heavy-ion reactions at relativistic bombarding energies offer a wide range of possibilities for studying multi-fragment decays of highly excited atomic nuclei. The largest fragment multiplicities measured so far were observed in central ^{197}Au on ^{197}Au collisions at a bombarding energy of 100 MeV per nucleon [26]. In these collisions the system of nearly 400 nucleons disintegrates completely into nuclear fragments and light particles. The analysis of the kinetic energy spectra in these reactions has re-

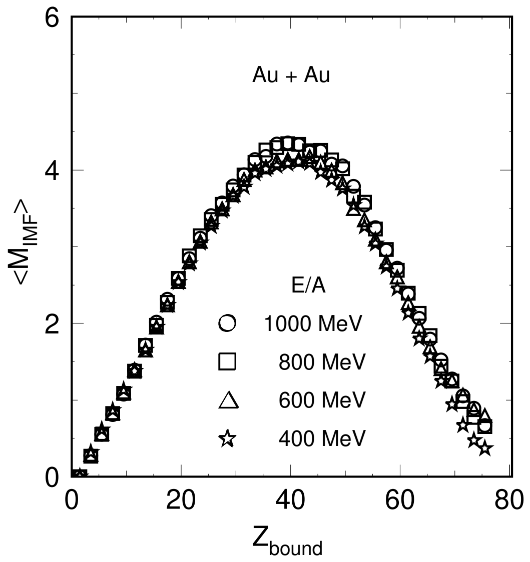

Figure 4: Mean IMF multiplicity $\langle M_{IMF}\rangle$ as a function of Z_{bound} for the reaction of ^{197}Au on ^{197}Au at E/A = 400, 600, 800, and 1000 MeV (from ref. [37]).

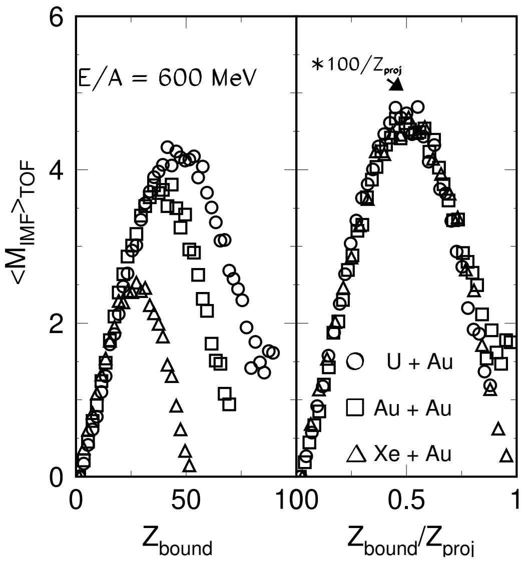

Figure 5: Left panel: Correlation between the mean multiplicity of intermediate-mass fragments $\langle M_{IMF}\rangle$ and Z_{bound} for the reactions ^{238}U on ^{197}Au (circles), ^{197}Au on ^{197}Au (squares), and ^{129}Xe on ^{197}Au (triangles) at E/A=600 MeV. Right panel: The same data as shown in the left panel, after dividing both observables by the respective projectile charge (from ref. [37]).

vealed a considerable collective outward motion superimposed on the random motion of the constituents at the breakup stage (radial flow) which represents up to one-half of the energy available in the center-of-mass frame [27]. This feature prevails, with monotonously increasing flow values, over the range of bombarding energies up to 1000 MeV per nucleon [28,29,30]. It demonstrates the strong dynamical coupling between entrance and exit channels in central collisions of heavy systems. Indeed, the process of fragment formation is found to be sensitive to the flow dynamics. The measured relative element yields are systematically correlated with the magnitude of the observed radial flow [30,31]. Within a coalescence picture, the suppression of heavier fragments for larger flow values may be caused by the reduction of the density in momentum space associated with the collective expansion [31].

While this interplay of dynamical and statistical effects in central collisions is currently a matter of high interest [32] and remains an interesting subject for future studies, we will focus in this report on multifragmentation processes in more peripheral nucleus-nucleus collisions at high energies. It will be shown, that the spectator systems formed during the initial stages of the reaction may also be excited to an extent that complete breakups can occur. Their invariant features are consistent with equilibration of the excited systems prior to their decay which justifies interpretations in statistical or thermodynamical terms.

The experimental setup (Fig. 3) resembles that used in earlier experiments but was modified in several respects: The solid angle adjacent to the acceptance of the ALADIN magnet was covered by the Catania hodoscope which consists of 84 Si-CsI(Tl) telescopes in closely packed geometry and which extends to angles up to $\Theta_{lab} \approx 16°$. The TP-MUSIC III served as the tracking detector. The multiple sampling of the ionization charges resulted in a resolution of $\Delta Z = 0.4$ (FWHM) for fragments with atomic number $Z \geq 8$. Lighter fragments were tracked and identified by collecting and amplifying their ionization charges with proportional counters mounted in three positions at the anode plane of the drift volume. The two-layered time-of-flight wall extended over a horizontal range of 2.4 m. The primary beam and projectile fragments emitted along directions close to that of the beam were detected with a plastic detector with light-fiber readout (denoted ZDF in Fig. 3). The large-area neutron detector LAND [33] was positioned close to zero degrees with respect to the incident beam direction and operated in a calorimetric mode.

The ALADIN spectrometer has been designed for optimum acceptance of projectile fragments which are focussed in forward directions. The focussing effect, however, is a function of the projectile velocity and changes with changing bombarding energy. We have, therefore, studied the extension of the projectile-spectator source in rapidity y and transverse momentum p_t both with experimental data and with model calculations. Guided by these analyses, we define the spectator source in rapidity by the condition $y \geq 0.75 \cdot y_{proj}$, where y_{proj} is the projectile rapidity, and by upper limits in the laboratory angle. The angular cuts were chosen inversely proportional to the projectile momentum. This was motivated by the observation that the widths of the transverse momentum distributions are independent of the bombarding energy. At the lower bombarding energies these angular cuts include some of the detectors of the Si-CsI(Tl) telescope array.

3 Universality of Spectator Decay

In contrast to central collisions, no apparent dependence on the entrance channel is observed in the decay of spectator nuclei produced in more peripheral collisions. The decay patterns were found to be mainly governed by the energy transfer to the spectator, as evident from the Z_{bound} scaling of the fragment charges and their correlations [34,35]. The quantity Z_{bound} is defined as the sum of the charges of all product nuclei with $Z \geq 2$ and is related to the energy deposit. When plotted as a function of this quantity the fragment multiplicities and correlations exhibit a universal behaviour. It was first observed as an invariance with respect to the chosen target in the decays of ^{197}Au projectiles at 600 MeV per nucleon [34,36].

In Fig. 4 the mean number of intermediate mass fragments (IMF's, $3 \leq Z \leq 30$) is shown as a function of Z_{bound} for the reaction of ^{197}Au on ^{197}Au at four bombarding energies. With the definition of the projectile spectator given above the correlation between the two quantities is seen to be independent of the projectile energy within the experimental accuracy. The maximum mean multiplicity of 4 to 4.5 fragments is reached at $Z_{bound} \approx 40$.

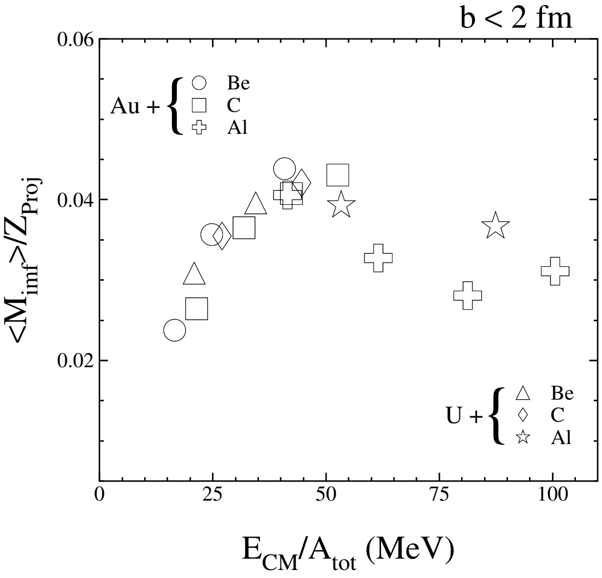

Figure 6: Mean IMF multiplicity $\langle M_{IMF} \rangle$ normalized to the projectile charge for central collisions – selected via Z_{bound} – between gold and uranium projectiles and light target nuclei ^{9}Be, ^{12}C, ^{27}Al as a function of available center-of-mass energy per nucleon (preliminary result from from ref. [39]).

The M_{IMF} versus Z_{bound} correlation depends on the mass of the projectile. Results obtained with three projectiles ^{129}Xe, ^{197}Au, and ^{238}U show that more fragments are produced in the decay of heavier projectiles (Fig. 5, left part). (Only fragments detected in the TOF-wall data were used for this comparison as the hodoscope was not in operation during the runs with the xenon beam.) However, a normalization with respect to the projectile charge reduces the three curves to a single universal relation (Fig. 5, right part). The observed invariance with respect to the entrance channel is not restricted to the multiplicity of intermediate-mass fragments but appears to be a very general feature of the relative asymmetries and other correlations between the abundancies and the atomic numbers of the fragmentation products [35,38].

This universality gives rise to the question as to where its limits may lie. Our data for collisions with rather light targets such as beryllium or carbon indicate that, in these cases, beam energies considerably above 400 MeV per nucleon are required in order to reach the maximum IMF production. Fig. 6 shows the mean fragment multiplicity – normalized with respect to the projectile charge number Z_{proj} – which is reached in the most central collisions as a function of the available center-of-mass energy per nucleon. For the beryllium target, for example, a beam energy of about 1 GeV per nucleon is necessary in order to reach the maximum normalized IMF multiplicity of about 0.04.

On the high-energy side, there is no limit known at present. Limiting fragmentation, i.e. a saturation of the production cross sections for intermediate mass fragments at bombarding energies in excess of several GeV, has been observed [40]. This suggests that the formation of spectator nuclei with high excitation energies may be common to heavy-ion collisions in the GeV range. A recent study of Jain *et al.* performed with ^{197}Au beams of 10.6 GeV per nucleon, available from the AGS at Brookhaven, and emulsion targets [41] reports nearly quantitative agreement with the fragmentation patterns of ^{197}Au on Cu collisions at 600 MeV per nucleon [34,35]. Note, that the latter data were obtained within the acceptance given by the TOF-wall of 1-m width. With respect to the more complete data presented here, the maximum number of intermediate-mass fragments of 3.5, reported by Jain *et al.*, is about one unit below the values from the present work, thus signaling an – albeit weak – beam energy dependence.

The fragmentation of ^{197}Au projectiles of 10.6 GeV per nucleon in collisions with emulsion targets was also investigated by the KLMM collaboration [42]. The Z_{bound} distributions reported for interactions with light targets (H,C,N, and O) resembles more closely the distribution measured for the ^{197}Au on Al rather than the ^{197}Au on C reaction at 600 MeV per nucleon. This may be considered as another indication for the role of the bombarding energy in reaching large cross sections for the high-multiplicity breakups in asymmetric systems.

4 Excitation Energies

The procedure used to determine the mass and excitation energy of the spectators prior to their decay is very similar to that proposed by Campi *et al.* [43]. However, besides the multiplicities and energies of charged particles and fragments those of free neutrons were also included in the analysis.
The basic idea is to determine the atomic number Z_0, the mass number A_0, and the excitation energy E_0 of the excited spectator from balance equations. Since the hydrogen isotopes were not detected assumptions concerning the overall N/Z ratio of the spectator, the intensity ratio of protons, deuterons, and tritons, and the kinetic energies of hydrogen isotopes had to be made. The mass numbers of He and Li fragments were obtained by randomly sampling the observed mass distribution. For simplicity, the mass numbers of heavier fragments were randomly chosen from mass distributions given by the semi-empirical EPAX parameterization [44] which was adjusted to the data of a previous study of Au+Pb reactions at E/A=600 MeV [45,46]. This simplification is justified since isospin correlations between coincident fragments were found to be small [45]. The uncertainties resulting from the variation of these quantities within reasonable limits are included in the adopted errors.

The results for the mass A_0 and the specific excitation energy E_0/A_0 are given in Fig. 7. The data points represent the results for individual bins in the Z_{max}-versus-Z_{bound} event representation. The mass A_0 decreases with decreasing Z_{bound} but, apparently, independent of Z_{max}. The smallest mean spectator mass in the bin of $Z_{bound} \leq 10$ is $\langle A_0 \rangle \approx 50$. Reconstructing the impact parameter from the quantity Z_{bound}, one finds that $\langle A_0 \rangle$ is remarkably well described by the simple participant-spectator geometry (see horizontal bars in Fig. 7).

The excitation energy E_0 appears to be a function of both Z_{bound} and Z_{max}; the higher values correspond to the smaller Z_{max} values, i.e. to more complete disintegrations of a system of given mass. The maximum number of fragments, observed

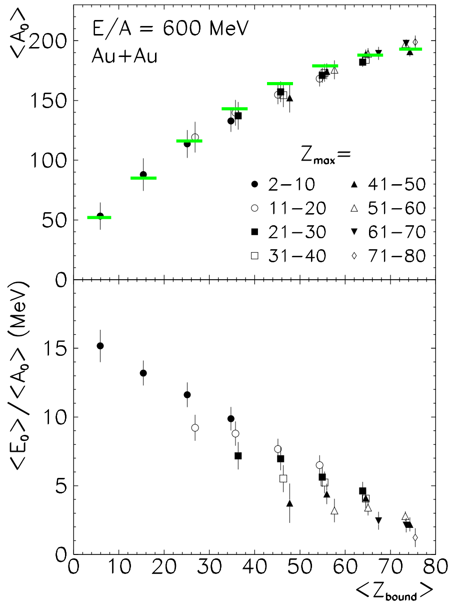

Figure 7: Average prefragment size $\langle A_0 \rangle$ and its excitation energy per nucleon $\langle E_0 \rangle / \langle A_0 \rangle$ as a function of Z_{bound} and different bins in Z_{max}.

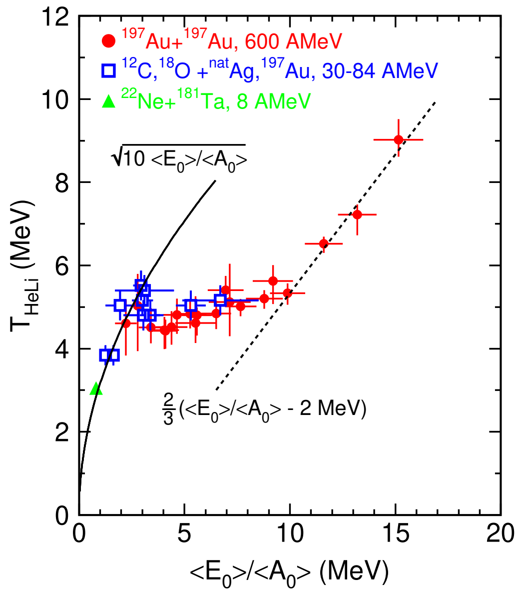

Figure 8: Caloric curve of nuclei determined by the dependence of the isotope temperature on the excitation energy per nucleon.

at $Z_{bound} \approx 40$, is associated with initial excitation energies of $\langle E_0 \rangle / \langle A_0 \rangle \approx 8$ MeV. With decreasing Z_{bound} the deduced excitation energies reach up to $\langle E_0 \rangle / \langle A_0 \rangle \approx 15$ MeV. These energy deposits for the range of small Z_{bound} are considerably larger than those obtained from the statistical analysis of the charge correlations of intermediate mass fragments ($Z \geq 3$) for ^{197}Au + Cu collisions at 600 MeV per nucleon [46].

5 The Isotope Thermometer

Less straight forward is the determination of a nuclear temperature. Nuclei are closed systems without an external heat bath. Consequently, the temperature of the system cannot be pre-determined but has to be reconstructed from observable quantities. For a microcanonical ensemble, the thermodynamic temperature T of a system with total energy E may be defined in terms of the total-energy state density $\Omega(E)$ via the relation

$$\frac{1}{T(E)} = \frac{\partial \left(ln\Omega(E) \right)}{\partial E}. \tag{1}$$

An experimental determination of the state density $\Omega(E)$ and its energy dependence is, however, hitherto impossible. Therefore, nuclear temperature determinations take recourse to 'simple' observables of a subsystem which constitute – at least for some ideal situations and generally within a canonical treatment – a good approximation to the true thermodynamic temperature. For example, for a nuclear system at low density and in chemical and thermal equilibrium a measure of the temperature T may be obtained via the double yield ratio of two isotope pairs, (Y_1/Y_2) and (Y_3/Y_4), differing by the same number of neutrons and/or protons [47]:

$$R = \frac{Y_1/Y_2}{Y_3/Y_4} = a \cdot e^{[(B_1-B_2)-(B_3-B_4)]/T}. \tag{2}$$

Here, B_i denotes the binding energy of particle species i and the constant a contains known spins and mass numbers of the fragments. Of course, a meaningful temperature scale can only be derived if the ratio R is sufficiently sensitive to the temperature of the system and if the yields of the considered fragments are measurable over a large range of excitation energy. A large sensitivity of this thermometer can be achieved if the constant $b = (B_1 - B_2) - (B_3 - B_4)$ is larger than the typical temperature to be measured.

Particularly large values for b are obtained if a $^3He/^4He$ ratio is involved. Indeed, the large cross section of He fragments as an abundant constituent in both the 'liquid' and the 'vapor' regime of nuclear systems *and* the strong binding energy of the α-particle is the lucky coincidence which is the basis of the temperature determination presented hereafter. In order to acquire for the second yield ratio also a sufficient production yield we define in the following a temperature $T_{HeLi,0}$ in terms of the yield ratios ^{3}He/^{4}He and ^{6}Li/^{7}Li

$$T_{HeLi,0} := 13.33/ln(2.18 \cdot \frac{Y_{6Li}/Y_{7Li}}{Y_{3He}/Y_{4He}}). \tag{3}$$

We note, that when using the d/t ratio rather than the ^{6}Li/^{7}Li ratio, a similar temperature scale, $T_{HHe,0}$, may be derived [47]. Whereas the d/t ratio was not accessible in the present experiment, $T_{HHe,0}$ may be more appropriate for central collisions.

Up to this point we considered nuclei in their ground state only and we ignored the effect of sequential decays during the final stage of the disassembly process. In particular, the yield of α-particles may be modified by secondary decays. (Note, however, that the effect of the α-feeding is partially neutralized by the feeding of ^3He.) In order to test the model dependence of the temperature definition via Eq. (3) and to investigate the influence of sequential decays we analyzed the fragment distributions predicted by several decay models.

Despite the strong feeding of the light particle yields through secondary decays, QSM calculations [49,50] predict an almost linear dependence of $T_{HeLi,0}$ on the actual temperature T of the system. For temperatures below 10 MeV, the ratio $T_{HeLi,0}$/T varies between about 0.95±0.05 and 0.75±0.05 for breakup densities between $0.1 \cdot \rho_0$ and $0.5 \cdot \rho_0$.

Results of sequential evaporation calculations with the code GEMINI [48] also confirm a nearly linear relation between $T_{HeLi,0}$ and the *initial* temperature of the system $T = \sqrt{k \cdot \langle E_0 \rangle / \langle A_0 \rangle}$, where k denotes the inverse level density parameter. In line with QSM calculations for higher densities the ratio $T_{HeLi,0}/T \approx 0.7$. Finally, the microcanonical multifragmentation model of Gross and co-workers [18] predicts also a rather constant ratio of 0.7 ±0.05 between $T_{HeLi,0}$ and the thermodynamic temperature of the system.

In order to account pragmatically for the systematic underestimation of the temperature by the quantity $T_{HeLi,0}$, we define the final isotope temperature via

$$T_{HeLi} = 1.2 \cdot T_{HeLi,0}. \qquad (4)$$

Thus, T_{HeLi} provides - within the models mentioned – a common temperature scale in the evaporation, the fragmentation as well as in the vapor regime of nuclear systems. (Clearly, a quantitative cross - calibration of this thermometer with other nuclear thermometers remains a primary task for future experiments.)

6 Nuclei Calorimetry

Figure 8 shows the isotope temperature as a function of the total excitation energy per nucleon. It is important to note that the isotope temperature and the excitation energy are practically independent observables, thus avoiding auto-correlations when plotted against each other. Excitation energy - temperature pairs of this caloric curve extracted for projectile spectators of Au+Au collisions at E/A=600 MeV are marked by the solid points. Data for target residues produced at intermediate energies between E/A=30 and 84 MeV are shown by the open squares. In the latter case, the excitation energies were also deduced from an energy balance [51] and T_{HeLi} was evaluated using the coincident light particle yields associated with emission from the target remnant [52]. The only values for T_{HeLi} in the evaporation regime below 2 MeV per nucleon excitation energy [53,54] is provided by the ^{22}Ne+^{181}Ta fusion reactions at E/A=8.1 MeV [55].

The caloric curve for spectator nuclei shown in Fig. 8 can be divided in three distinctly different sections. In line with previous studies in the fusion evaporation regime [53,54] the rise of T_{HeLi} for excitation energies below 2 MeV per nucleon is compatible with the low-temperature approximation of a fermionic system. Within the range of $\langle E_0\rangle/\langle A_0\rangle$ from 3 MeV to 10 MeV an almost constant value for T_{HeLi} of about 4.5-5 MeV is observed. This plateau may be related to the finding of rather constant emission temperatures over a broad range of incident energies which were deduced from the population of particle unstable levels in He and Li fragments [56]. We also note that the mean excitation energy of the plateau coincides with the limiting excitation energy for the fusion-evaporation process of about 4.5-6.4 MeV per nucleon [57]. Finally, beyond a total excitation energy of 10 MeV per nucleon, a steady rise of T_{HeLi} with increasing $\langle E_0\rangle/\langle A_0\rangle$ is seen which may be described by a linear relation

$$T_{HeLi} = 2/3 \cdot (\langle E_0\rangle/\langle A_0\rangle - 2MeV) \qquad (5)$$

where the slope of 2/3 alludes to a gas of classical, elementary particles. The onset of the vapor regime at an excitation energy per nucleon of about 10 MeV is also corroborated by a recent study of the INDRA group. For the system ^{36}Ar+^{58}Ni, they determined an *upper limit* of 52 MeV per nucleon for the beam energy which is necessary to reach a complete vaporization of the system into neutrons, H and He isotopes [58]. This beam energy converts to an available energy of about 12 MeV per nucleon in the total system.

7 Future Tasks

The qualitative similarity of the caloric curve of water and that of nuclei is striking. Yet it is clear, that this analogy should not be overemphasized and that the story is not over. A lot of work, both in experimental measurement and theoretical interpretation of the observed caloric curve, lies still ahead.

Different from bulk systems, nuclei are not confined by a constant external pressure. The dynamical evolution of the heated spectator nucleus will depend on its initial excitation energy and will, therefore, influence or even dominate the shape of the caloric curve. For illustration, the lines in Fig. 9 show the evolution of the sum of the thermal and potential energy of an isentropically expanding Fermi gas as a function of its density; the difference with respect to the initial energy at normal density (see numbers on the right hand side) corresponds to the energy stored (momentarily) in the collective expansive motion. For the low density equation-of-state of the finite nuclear system, a parabolic density dependence

$$(E/A)_{T=0} = K_c/18 \cdot (1 - \rho/\rho_0)^2 - 8MeV \tag{6}$$

with a compressibility $K_c = 144$ MeV was used [59]. Furthermore, we ignore any dissipative processes during the expansion.

For initial excitation energies below about 8 MeV per nucleon the system is not able to expand freely to zero density but will stop at a finite density before it collapses again. Since at the turning point the Coulomb barrier reaches its minimum value and since the system spends most of its time in this region, it is probably reasonable to assume that the fragmentation happens at this point. Indeed, the temperatures at the turning point lie, rather independent of the initial excitation energy, in the region of about 5 - 6 MeV.

For excitation energies beyond 8 MeV per nucleon, the system may energetically expand to zero density prior to its freeze-out. In such a case, the initial energy would be subdivided in a potential energy of 8 MeV per nucleon and a collective flow energy. In our experiment, we do, however, observe high temperatures in the gas phase of the caloric curve. These high values signal a freeze out at a finite density, which is not too surprising considering the finite range of the strong interaction and considering the fact that the expansion velocity is still moderate. Within the schematic picture shown in Fig. 9, the temperature of the gas branch of the caloric curve can be explained with a constant freeze-out density of about 15% of normal nuclear matter density.

While this interplay between the expansion dynamics and the density dependent properties of a Fermi gas might help to elucidate the gross features of the vapor branch one has to keep in mind that in this regime also typically 20% of the mass of the decaying system is contained in intermediate mass fragments. An internally consistent equation-of-state taking into account the clusterisation [63], the particle loss during the expansion [60,62], the viscosity of nuclear matter, and the systematic variation of the source size in peripheral collisions as well as the non-uniform, explosive initial flow in central collisions [62] is therefore required before more definite conclusions can be drawn. Nonetheless, if this scenario holds, the amount of radial motion which is transferred during the expansion into collective motion, will reflect both, the freeze-out density and the degree of dissipation during the expansion. Particle interferometry might provide another, independent, determination of the density of the system at freeze-out. A combination of these experimental informations might, therefore, allow a closer look at the expansion dynamics. Once we are able to control the amount of the non-thermal explosive flow in central collisions sufficiently well, this additional degree of freedom will enable us to explore the influence of the expansion dynamics in even further detail.

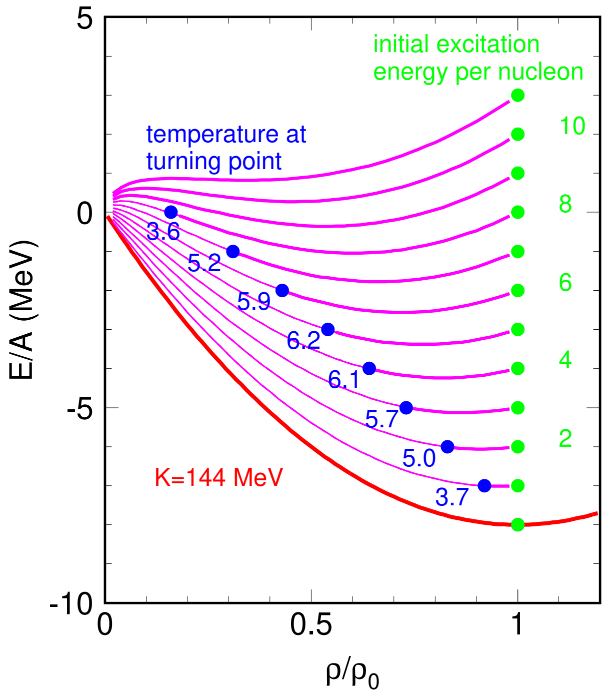

Figure 9: Evolution of an isentropically expanding Fermi gas in the energy per nucleon vs. density plane.

The plateau of the caloric curve is suggestive of a first-order phase transition with a substantial latent heat. It also seems to exclude - on first sight - the occurrence of a second-order phase transition which is the *sine qua non* for the determination of critical-point exponents [64,65]. For a finite system with N constituents a transition is, on the other hand, no longer characterized by a singular point but acquires a finite width over a temperature range ΔT_c around the transition temperature T_c. In case of a second order phase transition, $\Delta T_c/T_c$ is approximately given by $\Delta T_c/T_c \sim 1/\sqrt{N}$ [12]. For typical nuclear sizes of N≈100, the influence of a second order phase transition may, therefore, be perceptible at temperatures deviating by as much as 10% from the critical value. Furthermore, for a classical van der Waals gas the latent heat increases close to the critical point with $\sqrt{1-T/T_c}$ and reaches already at $T/T_c = 0.95$ values larger than $k_B T_c$. Thus, in finite systems typical features of a first-order phase transition - like a latent heat - and signals indicating the proximity of the critical point - like diverging moments - are not necessarily inconsistent, making the attempt to extract critical-point exponents – at least – a worthwhile and interesting venture.

All these open questions – and probably many more – will find their analogy in cosmology and high energy particle/nuclear physics, where the concept of *phase-transition* is equally important. In this respect, a deeper understanding of the liquid-gas phase transition of nuclei might also shed some light on the past history of our universe.

8 Acknowledgements

We thank J. Konopka for providing us with the results of the QSM calculations. J.P. and M.B. acknowledge the financial support of the Deutsche Forschungsgemeinschaft under the Contract No. Po256/2-1 and No. Be1634/1-1, respectively.

9 References

1. N.K. Glendenning, Phys. Rev. D **46**, 1274 (1992).
2. R. Tamagaki, Prog. Theor. Phys. Suppl. No. **112**, 1 (1993).
3. P.J. Siemens, Nucl. Phys. **A428**, 189c (1984).
4. D.Q. Lamb *et al.*, Phys. Rev. Lett. **41**, 1623 (1978).
5. H. Jaqaman, A.Z. Mekjian, and L. Zamick, Phys. Rev. C **27**, 2782 (1983) and Phys. Rev. C **29**, 2067 (1984).
6. P.J. Siemens, Nature **305**, 410 (1983).
7. J.E. Finn *et al.*, Phys. Rev. Lett. **49**, 1321 (1982).
8. A.D. Panagiotou *et al.*, Phys. Rev. Lett. **52**, 496 (1984).
9. N.T. Porile *et al.*, Phys. Rev. **C 39**, 1914 (1989).
10. X. Campi, Phys. Lett. **B 208**, 351 (1988).
11. X. Campi, J. Phys. A **19**, L917 (1986).
12. Y. Imry, Phys. Rev. B **21**, 2042 (1980).
13. P. Labastie and R.L. Whetten, Phys. Rev. Lett. **65**, 1567 (1990).
14. D.H.E. Gross, L. Satpathy, Meng Ta-chung, and M. Satpathy, Z. Phys. A **309**, 41 (1982).
15. S. Levit and P. Bonche, Nucl. Phys. **A437**, 426 (1985).
16. L. Satpathy, M. Mishra, and R. Nayak, Phys. Rev. C **39**, 162 (1989).
17. J. Bondorf *et al.*, Nucl. Phys. A **444**, 460 (1985).
18. D.H.E. Gross, Zhang Xiao-ze, and Xu Shu-yan, Phys. Rev. Lett. **56**, 1544 (1986); D.H.E. Gross, Prog. Part. Nucl. Phys. **30**, 155 (1993).
19. G. Bertsch and P.J. Siemens, Phys. Lett. **126B**, 9 (1983).
20. J.A. Lopez and P.J. Siemens, Nucl. Phys. **A431**, 728 (1984).
21. P.A. Hervieux and D.H.E. Gross, Z. Phys. D **33**, 295 (1995); D.H.E. Gross and P.A. Hervieux, Z. Phys. D (in print).
22. D.J. Wales and I. Ohmine, J. Chem. Phys. **98**, 7245 (1993).
23. H.-P. Cheng *et al.*, Phys. Rev. A **46**, 791 (1992).
24. A. Hüller, Z. Phys. B **93**, 401 (1994).
25. R. Blümel *et al.*, Nature **334**, 309 (1988).
26. M.B. Tsang *et al.*, Phys. Rev. Lett. **71**, 1502 (1993).
27. W.C. Hsi *et al.*, Phys. Rev. Lett. **73**, 3367 (1994).
28. W. Bauer *et al.*, Phys. Rev. C**47**, R1383 (1993).
29. S.C. Jeong *et al.*, Phys. Rev. Lett. **72**, 3468 (1994).
30. W. Reisdorf *et al.*, in *Proceedings of the International Workshop XXII, Hirschegg, 1994*, edited by H. Feldmeier and W. Nörenberg, p. 93.

31. G.J. Kunde *et al.*, Phys. Rev. Lett. **74**, 38 (1995).
32. J. Bondorf *et al.*, Phys. Rev. Lett. **73**, 628 (1994).
33. Th. Blaich *et al.*, Nucl. Instr. and Method **A314**, 136 (1992).
34. J. Hubele *et al.*, Z. Phys. A **340**, 263 (1991); Phys. Rev. C **46**, R1577 (1992);
35. P. Kreutz *et al.*, Nucl. Phys. **A556**, 672 (1993).
36. C.A. Ogilvie *et al.*, Phys. Rev. Lett. **67**, 1214 (1991).
37. A. Schüttauf, PhD-thesis University Frankfurt 1995 (unpublished).
38. A. Schüttauf *et al*, to be published.
39. W.D. Kunze, PhD-thesis University Frankfurt 1995 (unpublished).
40. S.B. Kaufman and E.P. Steinberg, Phys. Rev. C **22**, 167 (1980); R.E.L. Green and R.G. Korteling, Phys. Rev. C **22**, 1594 (1980).
41. P.L. Jain *et al.*, Phys. Rev. C **50**, 1085 (1994).
42. W.V. Jones *et al.*, Z. Phys. C **63**, 549 (1994).
43. X. Campi, H. Krivine, and E. Plagnol, Phys. Rev. C **50**, R2680 (1994).
44. K. Sümmerer *et al.*, Phys. Rev. C **42**, 2546 (1990).
45. V. Lindenstruth, PhD thesis, University Frankfurt 1993, GSI-report GSI-93-18 (unpublished).
46. A.S. Botvina *et al.*, Nucl. Phys. **A584**, 737 (1995).
47. S. Albergo *et al.*, Nuovo Cimento A **89**, 1 (1985).
48. R.J. Charity *et al.*, Nucl. Phys. **A483**, 371 (1988).
49. D. Hahn and H. Stöcker, Nucl. Phys. **A476**, 718 (1988).
50. J. Konopka *et al.*, Phys. Rev. C **50**, 2085 (1994).
51. R. Trockel *et al.*, Phys. Rev. C **39**, 729 (1989).
52. R. Trockel, PhD thesis, University of Heidelberg 1988 (unpublished).
53. G. Nebbia *et al.*, Phys. Lett. B **176**, 20 (1986).
54. D. Fabris *et al.*, Phys. Lett. B **196**, 429 (1987).
55. C. Borcea *et al.*, Nucl. Phys. **A415**, 169 (1984) and M.T. Magda, A. Pop and A. Sandulescu, Sov. J. Nucl. Phys. **43**, 753 (1986).
56. G.J. Kunde *et al.*, Phys. Lett. B **272**, 202 (1991).
57. W. Bohne *et al.*, Phys. Rev. C**41**, R5 (1990).
58. C.O. Bacri *et al.*, Institut de Physique Nucléaire Orsay pre-print, IPNO-DRE-95-10 (1995); A. Quatizerga, PhD thesis, Universite de Paris-Sud, Institut de Physique Nucléaire Orsay report, IPNO-T-95-05 (1995).
59. W.A. Friedman, 8-th Winter Workshop on Nuclear Dynamics, Jackson Hole, Wyoming, January 1992.
60. W.A. Friedman, Phys. Rev. C **42**, 667 (1990).
61. M. Belkacem, V. Latora, and A. Bonasera, Phys. Lett. B **326**, 21 (1994).
62. G. Papp and W. Nörenberg, Proceedings of the International Workshop XXII on Gross Properties of Nuclei and Nuclear Excitations, Hirschegg 1994, p. 87.
63. G. Peilert *et al.*, Phys. Lett. B **260**, 271 (1991).
64. M.L. Gilkes *et al.*, Phys. Rev. Lett. **73**, 1590 (1994).
65. J.B. Elliott *et al.*, Phys. Rev. C **49**, 3185 (1994).